Microstructure-Controlled Deposition of $SrTiO_3$ Thin Film on Self-Assembled Monolayers in an Aqueous Solution of $(NH_4)_2TiF_6$–$Sr(NO_3)_2$–H_3BO_3

Yanfeng Gao, Yoshitake Masuda, and Kunihito Koumoto*

Department of Applied Chemistry, Graduate School of Engineering, Nagoya University, Furo-cho, Chikusa-ku, Nagoya 464-8603, Japan

Received February 20, 2003. Revised Manuscript Received April 7, 2003

Strontium titanate precursor thin films were directly deposited on different self-assembled monolayers (SAM) in an aqueous solution at 40–60 °C. We have investigated the film growth rate, mechanism, and kinetics. The film microstructure and thickness can be controlled by appropriate SAM surfaces and solution conditions, such as the concentration of starting materials, pH, and deposition temperatures. Uniform, smooth, and adhesive films with thickness in the range of 25–480 nm could be successfully prepared on the OH surfaces of UV-modified SAM. The films were transparent and composed of closely packed particles of 20–50 nm, which formed by coalescence of very small particles. The Sr species preferably reacts with intermediate Ti species to produce $SrTiO_3$ precursor solid when the Sr and Ti species coexisted in the present solution system, resulting in a stoichiometry in terms of Sr/Ti ratio even if the Ti species was excessive.

1. Introduction

Much attention has been paid to the production of inorganic materials with specific size, orientation, and morphology because of the potential to design new materials and devices in various fields such as catalysis, medicine, electronics, ceramics, pigments, and cosmetics.[1–3] In the traditional ceramic process, powders with controlled shape, size, and size distribution are necessary to attain high-quality ceramics by optimizing their thermal, optical, mechanical, and electrical properties.[2] Control of size and its distribution is very important for nanomaterials, especially nanocrystals, because of their strongly size-dependent properties.[3] Compared to bulk ceramics, control of microstructures of thin film materials must be carried out in situ, that is, controlling should be conducted during film preparation.

Self-assembled monolayers (SAMs) have been employed to tailor morphology of thin films[4–12] or to control crystal nucleation.[13] SAMs are highly ordered and oriented molecular assemblies formed by the chemisorption of an active surfactant on a solid surface. SAMs can enhance heterogeneous nucleation,[14] increase interaction force such as electrostatic attraction between the SAM and particles generated in the solution,[15] and form oriented crystals.[13] The functional groups of SAMs themselves can be modified by different techniques such as X-ray,[16] electron beam,[16a,17] ion bombardment[18] and

* Corresponding author. Tel: 81-52-789-3327. Fax: +81-52-789-3201. E-mail: g44233a@nucc.cc.nagoya-u.ac.jp.

(1) (a) Archibald, D. D.; Mann, S. *Nature* **1993**, *364*, 430. (b) Mann, S.; Ozin, G. A. *Nature* **1996**, *382*, 313. (c) Yang, H.; Coombs, N.; Ozin, G. A. *Nature* **1997**, *386*, 692. (d) Li, M.; Schnablegger, H.; Mann, S. *Nature* **1999**, *402*, 393. (e) Yu, S.-H.; Cölfen, H.; Antonietti, M. *Chem. Eur. J.* **2002**, *8*, 2937.
(2) Santos, J. D.; Longo, E.; Leite, R. E.; Varela, J. A. *J. Mater. Res.* **1998**, *13*, 1152.
(3) (a) Peng, X. G.; Manna, L.; Yang, W. D.; Wickham, J.; Scher, E.; Kadavanich, A.; Alivisatos, A. P. *Nature* **2000**, *404*, 59. (b) Manna, L.; Scher, E. C.; Alivisatos, A. P. *J. Am. Chem. Soc.* **2000**, *122*, 12700. (c) Peng, Z. A.; Peng, X. G. *J. Am. Chem. Soc.* **2001**, *123*, 183. (d) Rao, C. N. R.; Kulkarni, G. U.; Thomas, P. J.; Edwards, P. *Chem. Eur. J.* **2002**, *8*, 29. (e) Chemseddine, A.; Moritz, T. *Eur. J. Inorg. Chem.* **1999**, 235. (f) Xia, Y.; Yang, P.; Sun, Y.; Wu, Y.; Mayers, B.; Gates, B.; Yin, Y.; Kim, F.; Yan, H. *Adv. Mater.* **2003**, *15*, 353.
(4) Koumoto, K.; Seo, S.; Sugiyama, T.; Seo, W. S.; Dressick, W. J. *Chem. Mater.* **1999**, *11*, 2305.
(5) Masuda, Y.; Jinbo, Y.; Yonezawa, T.; Koumoto, K. *Chem. Mater.* **2002**, *14*, 1236.
(6) (a) Koumoto, K.; Masuda, Y.; Wang, D. J. *Int. J. Soc. Mater. Eng. Resour.* **2002**, *10*, 49. (b) Masuda, Y.; Sugiyama, T.; Lin, H.; Seo, W. S.; Koumoto, K. *Thin Solid Films* **2001**, *382*, 153. (c) Wang, D. J.; Masuda, Y.; Seo, W. S.; Koumoto, K. *Key Eng. Mater.* **2002**, *214–215*, 163.
(7) (a) Saito, N.; Haneda, H.; Sekiguchi, T.; Ohashi, N.; Sakaguchi, I.; Koumoto, K. *Adv. Mater.* **2002**, *14*, 418. (b) Shirahata, N.; Masuda, Y.; Yonezawa, T.; Koumoto, K. *Langmuir* **2002**, *18*, 10379.
(8) Xu, D.; Kang, E. T.; Neoh, K. G.; Zhang, Y.; Tay, A. A. O.; Ang, S. S.; Lo, M. C. Y.; Vaidyanathan, K. *J. Phys. Chem. B* **2002**, *106*, 12508.
(9) Nagtegaal, M.; Stroeve, P.; Ensling, J.; Gütlich, P.; Schurrer, M.; Voit, H.; Flath, J.; Käshammer, J.; Knoll, W.; Tremel, W. *Chem Eur. J.* **1999**, *5*, 1331.
(10) Niessen, T. P.; De Guire, M. R. *J. Electroceram.* **2001**, *6*, 169.
(11) Niessen, T. P.; Bill, J.; Aldinger, F. *Chem. Mater.* **2001**, *13*, 1552.
(12) Pizem, H.; Sukenik, C. N.; Sampathkumaran, U.; McIlwain, A. K.; De Guire, M. R. *Chem. Mater.* **2002**, *14*, 2476.
(13) (a) Aizenberg, J.; Black, A. J.; Whitesides, G. M. *Nature* **1999**, *398*, 495. (b) Aizenberg, J.; Black, A. J.; Whitesides, G. M. *J. Am. Chem. Soc.* **1999**, *121*, 4500.
(14) (a) Tarasevich, B. J.; Rieke, P. C. *Chem. Mater.* **1996**, *8*, 292. (b) Rieke, P. C.; Wiecek, R.; Marsh, B. D.; Wood, L. L.; Liu, J.; Song, L.; Fryxell, G. E.; Tarasevich, B. J. *Langmuir* **1996**, *12*, 4266.
(15) Shin, H.; Agarwal, M.; De Guire, M. R.; Heuer, A. H. *Acta Mater.* **1998**, *46*, 801. (b) Aizenberg J.; Braun P. V.; Wiltzius, P. *Phys. Rev. Lett.* **2000**, *84*, 2997.
(16) (a) Zharnikov, M.; Grunze, M. *J. Vac. Sci. Technol. B* **2002**, *20*, 1793. (b) Wagner, A. J.; Carlo, S. R.; Vecitis, C.; Fairbrother, D. H. *Langmuir* **2002**, *18*, 1542. (c) Wagner, A. J.; Han, K. P.; Vaught, A. L.; Fairbrother, D. H. *J. Phys. Chem. B* **2000**, *104*, 3291. (d) Carlo, S. R.; Wagner, A. J.; Fairbrother, D. H. *J. Phys. Chem. B* **2000**, *104*, 6633.
(17) Mino, N.; Ozaki, S.; Ogawa, K.; Hatada, M. *Thin Solid Films* **1994**, *243*, 374.

10.1021/cm030234s CCC: $25.00 © 2003 American Chemical Society
Published on Web 05/17/2003

UV irradiation.[19,20] Therefore, a variety of surfaces with specific interactions can be produced with fine chemical control, enabling control of film formation and manipulation of morphology. We found that thin films can be selectively produced on the hydrophilic surfaces of silanol regions that were prepared by UV irradiation of SAMs; films in these regions were uniform and showed strong adherence to the substrates.[4−6,21−23] However, a hydrophobic SAM surface such as octadecyl-trichlorosilane (OTS) dramatically suppressed film formation. It is possible that no deposit is formed in the very beginning stage of soaking before a dense film is generated on the silanol region.[5,6,22−24] In some cases, deposition occurred on both hydrophilic and hydrophobic regions, but the film on the latter surfaces was too weak to be easily peeled off by ultrasonication.[4] These differences enable us to produce micropatterns of functional ceramic films and meanwhile control their morphologies to some degree.

Other research studies on the effects of SAMs on film morphology have been reported, but few are systematic. Niesen et al.[11] recently reported a novel method for deposition of TiO_2 thin films by a peroxide route on different self-assembled monolayers. Uniform titania films formed on sulfonated SAMs, whereas hydroxyl and amine functionalities led to inhomogeneous coatings. Pizem et al.[12] carried out relatively concrete studies on the effects of surface functionality on solution-deposited titania films. Different sulfonated surfaces and variously prepared silicon wafers were employed to deposit TiO_2 thin films by the liquid-phase deposition (LPD) method. The influence of surfaces on the growth rate, film thickness, and mechanism were discussed, but morphology characteristics were not yet systemized. We micropatterned TiO_2 thin films in a Ti-species-containing organic solution on the different SAMs; the resolution of micropatterns can be improved through controlling the reactivity on the different regions by changing functional groups of starting materials and/or SAMs; changes in the film morphology with changes in starting materials were also investigated, and a smooth film on the OTS-derived silanol surface was obtained by depositing in an $TiCl_4$-toluene solution.[5] However, the effect of the functional groups themselves on the morphology of TiO_2 films is still unclear.

We developed a unique chemical solution method and successfully deposited strontium titanate ($SrTiO_3$; STO) precursor solid thin films on both the UV-modified self-assembled monolayers (SAMs)[23] and silicon substrates[25] by the LPD method. Growth of the STO precursor solid thin film was promoted by using the UV-modified SAM surface. This simple method enabled us to deposit the STO precursor solid thin films directly in a $Sr(NO_3)_2$/$(NH_4)_2TiF_6$/H_3BO_3 aqueous solution at an ambient temperature. The as-deposited thin film demonstrated stoichiometric composition of Sr/Ti and contained fluorine as a main impurity, which was eliminated by annealing at 500 °C for 2 h in air. The interesting stoichiometric composition of our films is significant because it makes it possible to avoid the problematic effects of nonstoichiometry on the dielectric properties. Comparably, Lee et al. has reported direct deposition of a thin film containing Ba, Ti, and O by the LPD method using an aqueous solution of barium fluorotitanate.[26] However, the chemical composition of the film was nonstoichiometric, typically Ba/Ti/O 1:10.9:16.5.[26] Annealing our as-deposited thin films at 500 °C not only eliminated the impurity of fluorine (checked by XPS), but also crystallized the amorphous thin films to perovskite-type STO. XPS results showed that the amount of residual carbon was lower than that of sol−gel-derived thin films, which are usually synthesized by using alkoxides as starting materials. The crystallized temperature of 500 °C is much lower than that of the perovskite-type solids synthesized by some newly developed wet-chemical methods.[27] Current−voltage and capacitance−voltage characteristics of metal-oxide-semiconductor (MOS) devices using our as-deposited thin film and those annealed as the gate films revealed that our STO thin film is promising for dielectric applications.

To apply our STO thin films to microelectronics, the microstructure of the film should be well controlled. The STO thin film prepared by the present method shows particulate characteristics, and hence, control of particle sizes is important to manipulate a series of properties of thin film. Both grains and grain boundaries play an important role in many electroceramic applications. The grain boundaries of STO-based varistors can be insulated through a diffusion process of specific oxides, exhibiting high resistivity. They also act as fast transport paths and result in high leakage current when the film is used as a gate dielectric for the MOS device.[28] Control of particle size and its aggregation is one effective way to control and design grain size and boundaries, and it is also important to attain high-density thin films exhibiting improved dielectric properties. The mean particle size also dominates the minimum thickness of the film with 100% coverage, which will confine the application of our STO thin films to some thickness-limited devices, i.e., gate oxide layers of the MOS device, which need the film thickness less than 10 nm. In addition, the surface roughness is also a key characteristic for thin film materials, especially

(18) (a) Evans, C.; Wade, N.; Pepi, F.; Strossman, G.; Schuerlein, T.; Cooks, R. G. *Anal. Chem.* **2002**, *74*, 317. (b) Shen, J. W.; Grill, V.; Evans, C.; Cooks, R. G. *J. Mass Spectrom.* **1999**, *34*, 354. (c) Cyganik, P.; Postawa, Z.; Meserole, C. A.; Vandeweert, E.; Winograd, N. *Nucl. Instrum. Methods B* **1999**, *148*, 137.

(19) (a) Saito, N.; Hayashi, K.; Sugimura, H.; Takai, O. *J. Mater. Chem.* **2002**, *12*, 2684. (b) Yang, Z. P.; Frey, W.; Oliver, T.; Chilkoti, A. *Langmuir* **2000**, *16*, 1751. (c) Hutt, D. A.; Cooper, E.; Leggett, G. J. *J. Phys. Chem. B* **1998**, *102*, 174. (d) Dressick, W. J.; Dulcey, C. S.; Georger, C. H.; Calvert, J. M. *Chem. Mater.* **1993**, *5*, 148. (e) Jennane, J.; Boutros, T.; Giasson, R. *Can. J. Chem.* **1996**, *74*, 2509.

(20) (a) Dressick, W. J.; Calvert, J. M. *Jpn. J. Appl. Phys.* **1993**, *32*, 5829, and references therein. (b) Dressick, W. J.; Dulcey, C. S.; Chen, M.-S.; Calvert, J. M. *Thin Solid Films* **1996**, 284−285, 568.

(21) Masuda, Y.; Seo, W. S.; Koumoto, K. *Langmuir* **2001**, *17*, 4876.

(22) Gao, Y.; Masuda, Y.; Yonezawa, T.; Koumoto, K. *J. Ceram. Soc. Jpn.* **2002**, *110*, 379.

(23) Gao, Y.; Masuda, Y.; Yonezawa, T.; Koumoto, K. *Chem Mater.* **2002**, *14*, 5006.

(24) Masuda, Y.; Sugiyama, T.; Koumoto, K. *J. Mater. Chem.* **2002**, *12*, 2643.

(25) Gao, Y.; Masuda, Y.; Yonezawa, T.; Koumoto, K. *Mater. Sci. Eng. B*, in press.

(26) Lee, M. K.; Tung, K. W.; Cheng, C. C.; Liao, H. C.; Shih, C. M. *J. Phys. Chem. B*, **2002**, *106*, 4963.

(27) (a) Camargo, E. R.; Kakihana, M. *J. Am. Ceram. Soc.* **2002**, *85*, 2107. (b) Camargo, E. R.; Kakihana, M. *Chem. Mater.* **2001**, *13*, 1181. (c) Camargo, E. R.; Popa, M.; Frantti, J.; Kakihana, M. *Chem. Mater.* **2001**, *13*, 3943.

(28) (a) Kilingon, I.; Maria, J.-P.; Streiffer, S. K. *Nature* **2000**, *406*, 1032. (b) Wilk, G. D.; Wallace, R. M.; Anthony, J. M. *J. Appl. Phys.* **2001**, *89*, 5243.

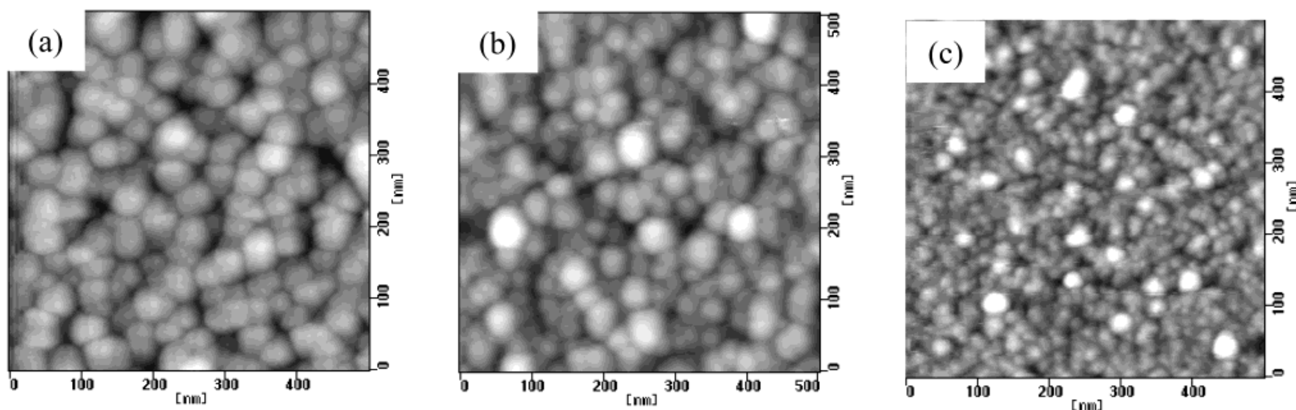

Figure 1. AFM images of STO precursor thin films deposited in an aqueous solution containing 25 mM AHFT, 25 mM SN, and 75 mM BA on OTS-derived silanol surfaces at different temperatures for 2 h: 40 °C (a), 50 °C (b), and 60 °C (c).

for ultrathin films. Flat surfaces will improve the interface quality between thin film and electrode. In the present study, we focused on control of film morphology by selecting appropriate SAMs and optimizing deposition conditions. A comparative study on deposition of TiO_2 and STO by the LPD method was conducted, and control of STO film composition in stoichiometry (Sr/Ti = 1) was also discussed.

2. Experimental Section

SAM Preparation and Modification. P-type Si (100) wafers (Shinetsu; resistivity 5−10 Ωcm) employed for the substrates, were cleaned ultrasonically in acetone, ethanol, and deionized water (>17.6 MΩcm), followed by immersion in boiling water for 5 min. After drying at 50 °C in air, the substrate was exposed to UV light for 2 h. SAM materials were heptadecafluoro-1,1,2,2,-tetrahydrodecyltrichlorosilane (HFDTS, Aldrich, Milwaukee, WI), octadecyl-trichloro-silane (OTS, Acros, NJ), and phenyltrichlorosilane (PTCS, Aldrich). SAMs were prepared by immersing the cleaned and dried substrate into an anhydrous toluene (99.8%, water < 0.002%, Aldrich) solution containing 1% vol SAM materials for 5 min under an N_2 atmosphere. After being dried under the N_2 atmosphere, the substrates with SAMs were then baked at 120 °C for 5 min to remove residual solvent and to promote chemisorption of the SAMs.

For transformation of SAM functionality, HFDTS−, PTCS−, or OTS−SAMs were exposed for 2−3 h to UV light (centered at 253 nm) from a low-pressure Hg lamp (5 W × 4 Hg lamps, NL-UV253, Nippon Laser & Electronics Lab), which modified the functional groups of the exposed areas and resulted in the photocleavage of the original hydrophobic groups. Water-drop contact angle measurement (CA-D, Kyowa Interface Sci.) and XPS analysis (ESCA-3200, Shimadzu; pass energy 75 eV) were conducted to check the successful formation of SAMs and the photocleavage of functional groups by UV irradiation.

Deposition of STO Films. Ammonium hexafluorotitanate [$(NH_4)_2TiF_6$ (AHFT), 98.5%, Mitsuwa Chemical Co., Japan], boric acid (BA), strontium nitrate (SN) (purity 98%, Kishida Chemical Co., Japan), and diluted water were employed for the starting materials. Both reagents were used in the as-received forms without further purification. They were separately dissolved in diluted water and then mixed to form a homogeneous solution containing 25 mM AHFT, 25 mM SN, and 0−75 mM BA. The typical molar ratio was AHFT/SN/BA 1−2:1−2:3. The pH of the solution was 3.4, unless especially noted. The deposition of a solid phase was conducted by immersing the patterned SAM-covered substrate into the solution at 50 °C for 0.5−24 h. The substrate was floated on the surface of the solution with the SAM side upside down to prevent particles formed in the solution from accumulating on the substrate surface. The substrate with a deposit was rinsed carefully in distilled water before air-drying.

Characterization Techniques. A scanning electron microscope (SEM; model S-3000N, Hitachi) and a field emission SEM (FE-SEM; JSM-6330F) were used to observe the deposits and precipitates on the substrate. A scanning probe microscope (SPI3800N, Seiko Instruments Inc.) was operated in AFM contact mode to observe the topography of the films; a triangular-shaped Si_3N_4 cantilever (NP-S, Nanoprobes Digital Instruments Inc.) was used; and scans were carried out at room temperature under ambient air with a frequency of 1−2 kHz. The structure and phase composition were characterized by X-ray diffraction (XRD; model RAD-1C, Rigaku; 40 kV, 30 mA) with Cu Kα radiation (λ = 0.15418 nm) at a scanning speed of 1°/min. The thickness of films was measured by a laser ellipsometer (PZ2000, Philips) with an incidence angle of 70° and wavelength of 632.8 nm. The zeta potential of the as-obtained powders was measured (ZETASIZER $3000HS_A$, Malvern Instruments, U.K.) by dissolving a trace of powder in 50 mL of deionized water.

3. Results

Effect of Solution Temperature on the Microstructure. Hereafter, AHFT, SN, and BA refer to ammonium hexafluorotitanate, strontium nitrate, and boric acid, respectively. The pH of the solution was 3.4, unless otherwise noted. Figure 1 shows AFM images of STO precursor thin film deposited on the OTS-derived silanol surfaces at 40−60 °C for different soaking times. All films were composed of closely packed particles of 15−30 nm diameter; the particle size decreased with increasing solution temperature. The statistic root-mean-square (RMS) roughness for the entire measured area (500 × 500 nm^2) was 2−7 nm, which tended to decrease with prolonging soaking time at corresponding temperatures, respectively. It is possible that the particles preferred to attach to the grain boundary by homogeneous joint growth, decreasing the contrast between grain and boundary and presenting a smooth surface.

Effect of Various SAMs on the Microstructure. Figure 2 shows particle sizes (observed by AFM) and RMS roughnesses of thin films deposited at 50 °C on the PTCS or OTS along with their derived silanol surfaces. The particle sizes were about 33 nm on the OTS-derived silanol surfaces, 30 nm on the OTS surfaces, 23 nm on the PTCS-derived silanol surfaces, and 16 nm on the PTCS surfaces, respectively. Moreover, the particle size did not increase, and was independent of the soaking time. Films on the PTCS surfaces were observed to have smaller particles than those on the other surfaces; generally, the particle size was much

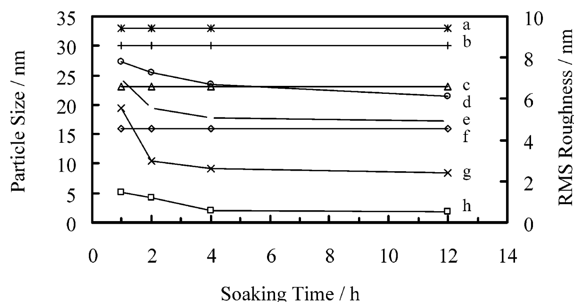

Figure 2. Particle sizes (a, b, c, f; observed by AFM) and RMS roughnesses (d, e, g, h) of STO precursor thin films deposited in an aqueous solution containing 25 mM AHFT, 25 mM SN, and 75 mM BA at 50 °C for different times on the different surfaces: (a) and (e) silanol surface derived from OTS; (b) and (d) OTS surface; (c) and (g) silanol surface derived from PTCS; and (f) and (h) PTCS surface.

smaller than that of PTCS- or OTS-derived silanol surfaces. Grain boundaries became blurred when the deposition proceeded and STO thin films with flat surfaces were achieved. RMS of the measured area (500 $\times$ 500 nm^2) for the thin film obtained by deposition for 4 h on the PTCS surface was as small as 0.6 nm, which is almost the same as that for the SAM-covered substrate.

Effect of Amount of Boric Acid. Figure 3 shows AFM images of films deposited in the 0.025 M AHFT/SN aqueous solutions at 60 °C with different amounts of BA. The results indicate that a much longer induction time was necessary for precipitate formation when the amount of boric acid was decreased. For AHFT/SN/BA 1:1:3, a dense thin film could be obtained after soaking for 1 h (AFM image not shown here). Films obtained after depositing for 5, 6, and 12 h are shown in Figure 3 panels A1, A2, and A3, respectively. When the molar ratio of AHFT/SN/BA was reduced to 1:1:1, obvious deposits could be observed after soaking for 5 h (Figure 3 B1), and grain number densities increased after soaking for 6 h (Figure 3 B2) and 7 h (result not shown). Dense film could not be obtained until deposition for 8 h. An image of relatively dense film (after soaking for 12 h) is shown in Figure 3 B3, while particle size was found to be much larger than that obtained at SN/AHFT/BA 1:1:3, implying that a greater number of nuclei had formed with increasing amount of BA. The increase in the particle size with soaking time is obvious when the relative quantity of boric acid was reduced, suggesting that the initially formed grains further grew larger under relatively low supersaturation.

The growth kinetics was further investigated by cross-sectional SEM observation. Hemisphere-shaped grains can be observed in the initial stages (Figure 3 C1 and C2), and a columnar film with a thickness of 450 nm was produced after soaking for 12 h (Figure 3 C3). In

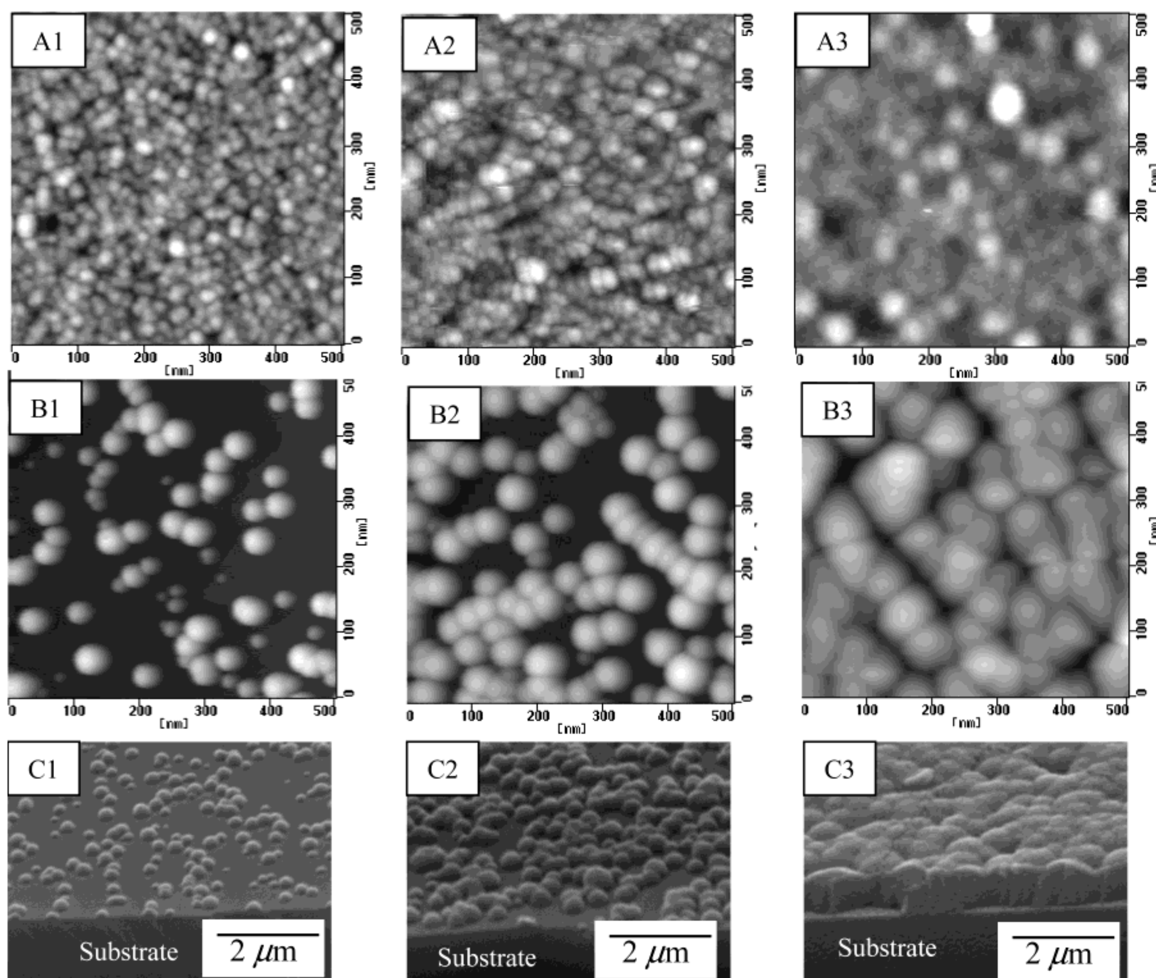

Figure 3. AFM images of STO precursor thin films deposited at 60 °C in aqueous solutions with a molar ratio of AHFT/SN/BA 1:1:3 for 5 h (A1), 6 h (A2), and 12 h (A3); AHFT/SN/BA 1:1:1 for 5 h (B1), 6 h (B2), and 12 h (B3); along with corresponding SEM photographs C1, C2, and C3. Samples were tilted 60°.

fact, a FE-SEM cross-sectional photograph (see Figure 6 later in this paper) shows that the columnar characteristic of the cross-sectional surface itself is also composed of small grains.

Effect of Solution pH. The samples were prepared by keeping the molar ratio of AHFT/SN/BA 1:1:3, reducing the pH by the addition of an appropriate amount of HNO_3 (Kishida Chem.; 1 M; the pH was accurately measured by a pH meter (pH meter F-21, Horiba)), then floating the substrate on the surface of the solution with the SAM surface upside down at 50 °C for various periods of time. For solutions with the initial pH of 3.40, 3.2, 3.0, and 2.8, the pH after soaking for 21 h changed to 3.35, 2.40, 2.35 and 2.23, respectively. The obvious change in the pH occurred after deposition of thin films when the initial pH was less than 3.2.

The influence of pH on the microstructure of STO thin films is shown in Figure 4. Slightly reducing the pH of the solution resulted in not only prolonging the induction time but also the formation of an unknown crystalline solid. This solid is not STO but could transform to STO after annealing at 600 °C in air. Unlike other films, films obtained under the present conditions did not exhibit mirrorlike surfaces. Moreover, dramatic changes in morphology occurred: closely packed brush-like aggregates of crystalline fibers were produced in the initial stage. These bundles grew further by attachment to unexpected cone-like structures with remarkable self-similarity. The fiber texture of the crystal is related to the anisotropic characteristic of crystal growth rate; growth predominantly progresses in specific directions. From the viewpoint of thermodynamics, the entropy of such a self-assembled structure should be maximized by minimizing the excluded volume per fibers. This morphology was also observed for the deposits on the OTS surface (photograph not shown), but not observed for the precipitate in the bottom of solution (photograph not shown). Hence, we infer that nucleation depends on the substrate to some degree.

Whether or not the structure is composed of single fibers cannot be confirmed by the current SEM photographs, but we can infer that the present condition was effective for one-dimensional crystallization, and that the crystals preferentially attached themselves in the perfect vectorial orientation of the building blocks; that is, there is no obviously transnational or rotational disorder between these blocks. Although crisscrossing occurred in the observed area, it is clear that the fiber bundles, along with cone-like superstructures, were generated from a single point of the substrate; that is, nucleation occurred against a substrate, indicating heterogeneous nucleation and growth process. The growth of the fiber bundles based on surface-promoted heterogeneous nucleation and formation of cone-like superstructures suggests that the density of the film should be much lower in these cases.

4. Discussion

Difference in Deposition Behavior between STO and TiO_2 Thin Films by the LPD Method. XRD results show that all as-deposited STO precursor thin films except those synthesized at low pH conditions were amorphous, which differs from TiO_2 thin films prepared by the controlled-hydrolysis method. The hydrolysis of $TiCl_4$,[11,29] TiF_4,[30] or $(NH_4)_2TiF_6$[4,12,24,31] can yield either amorphous or crystallized TiO_2 thin films depending on the synthetic conditions employed. Solutions with both lower titanium concentrations and ligands, such as F^-, SO_4^{2-}, and urea (H_2NCONH_2) that coordinate strongly to titanium, usually favor the formation of crystallized TiO_2 thin films.[12] However, these conditions are not sufficient for crystallization considering that only amorphous STO precursor thin films could be deposited under most of our conditions.

The second difference between LPD-derived-TiO_2 and STO film lies in their thickness and growth rate. When maintaining AHFT/BA 1:3 for both deposition of TiO_2 and STO thin film, in the case of room-temperature deposition of TiO_2, deposition proceeded for at least 73 h (initial pH 3.88) at a growth rate of 5−7 $nm\cdot h^{-1}$ using an oxidized, hydrolyzed silicon substrate, producing a film with a maximum thickness of 570 nm.[12] Deki et al.[31] found that deposition continued up to 80 h at an almost constant growth rate (5−25 $nm\cdot h^{-1}$ depending on the deposition solution) and a film with a maximum thickness of 800 nm could be fabricated on the glass without a SAM. When using functional surfaces and raising the solution temperature to 50 °C, Pizem et al.[12] reported a much higher growth rate of 70 $nm\cdot h^{-1}$ and a film over 1000 nm thick was prepared. In the case of LPD-prepared STO thin film, we obtained growth rates of 60−100 $nm\cdot h^{-1}$ for the first 2 h at 50−60 °C, dropping to 30−60 $nm\cdot h^{-1}$ beyond 2 h. After 5 h, almost no obvious increase in the film thickness was observed. Thickness of a film with 100% coverage obtained by deposition for 1−24 h ranged from 100 to 480 nm on the SAM-derived silanol surfaces. By prolonging soaking time to 40 h, films with gray-white surfaces (compared to the mirrorlike surfaces for 24 h deposition) could be prepared when they were dried at room temperature, indicating that the film thickness increased, but peeling also occurred because of the residual stress generated during drying. For deposition of STO precursor thin films, the growth rate in the first 2 h was higher than that for the TiO_2 thin film deposited on a highly hydrophilic sulfonated surface by the LPD method,[12] but the possible maximum thickness of the STO precursor thin film with strong adhesion to the substrate was much thinner than that of TiO_2 (450 nm vs 1000 nm).

The third difference lies in the different effects of pH on the deposition of TiO_2 and STO. As will be discussed later, formation of both STO and TiO_2 is associated with the hydrolysis reaction of AHFT, which is an acid-generation reaction. Reducing the pH of the initial solution can suppress the acid generation, restricting the corresponding reaction. The similar result has been obtained in the preparation of TiO_2.[4,12] However, a high-quality TiO_2 thin film could still be produced by prolonging the soaking time. In the presence of stron-

(29) (a) Kavan, L.; Rathousky, J.; Gratzell, M.; Shklover, V.; Zukal, A. *J. Phys. Chem. B.* **2000**, *104*, 12012. (b) Zheng, Y.; Shi, E.; Chen, Z.; Li, W.; Hu, X. *J. Mater. Chem.* **2001**, *11*, 1547. (c) Cheng, H.; Ma, J.; Zhao, Z.; Qi, L. *Chem. Mater.* **1995**, *7*, 663. (d) Harada, H.; Ueda, T. *Chem. Phys. Lett.* **1984**, *106*, 229.

(30) (a) Shimizu, K.; Imai, H.; Hirashima, H.; Tsukuma, K. *Thin Solid Films* **1999**, *351*, 220. (b) Imai, H.; Matsuda, M.; Shimizu, K.; Hirashima, H.; Negishi, N. *J. Mater. Chem.* **2000**, *10*, 2005.

(31) Deki, S.; Aoki, Y.; Hiroi, O.; Kajinami, A. *Chem. Lett.* **1996**, 433.

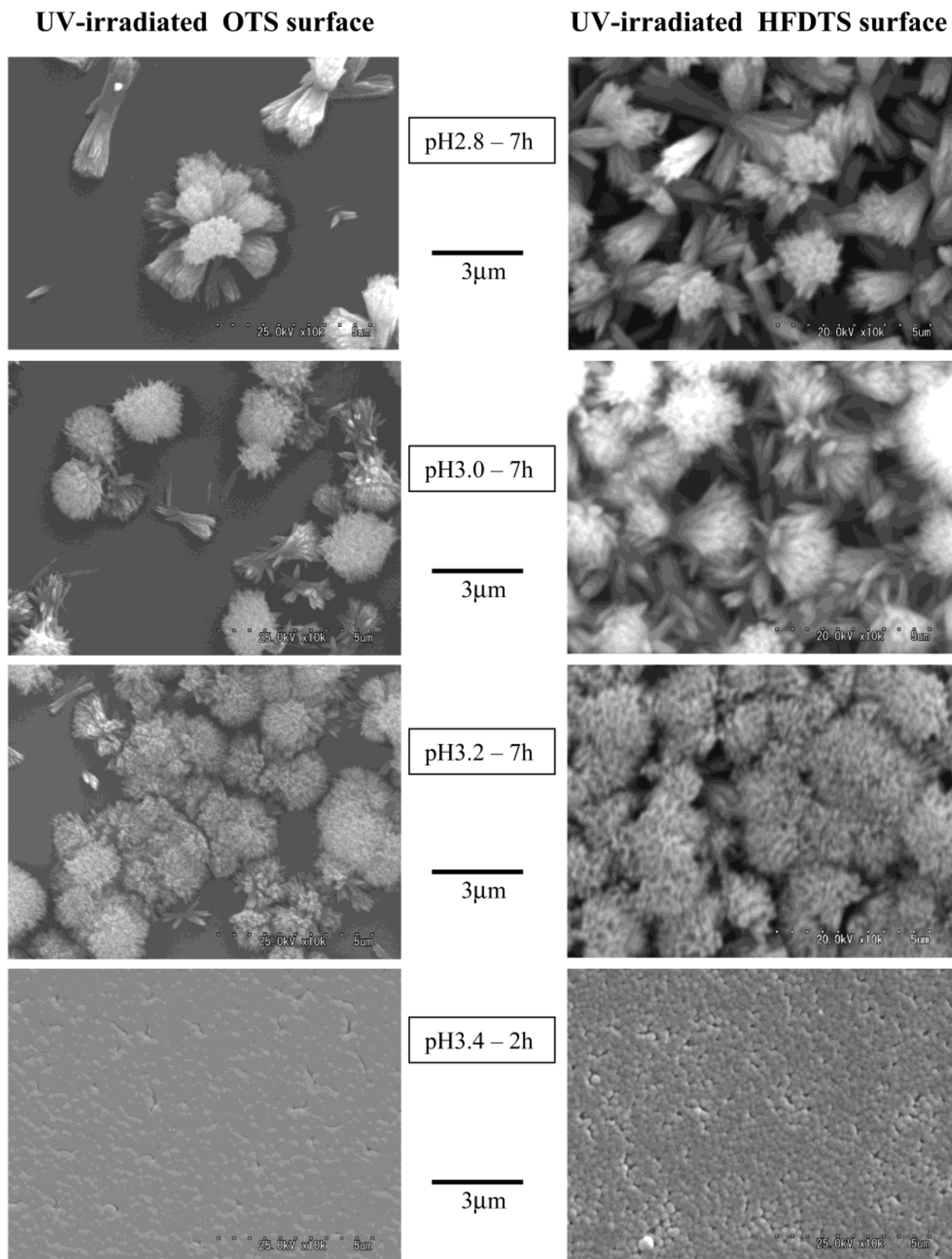

Figure 4. SEM photographs of STO precursor thin films deposited in an aqueous solution containing 25 mM AHFT, 25 mM SN, and 75 mM BA at 50 °C under different pH conditions; SAMs are UV-irradiated OTS and HFDTS, respectively.

tium species, fiberlike crystals were formed, and we cannot attain a dense thin film even after soaking for as long as 21 h.

Control of Chemical Composition. Without $Sr(NO_3)_2$, the solution of AHFT and boric acid was visually clear within 2 h (pH 2.88, 50 °C),[12] which is

much longer than that in the deposition of STO films under similar conditions. A pure AHFT aqueous solution could stay transparent for several months, whereas a mixture of equimolar SN and AHFT aqueous solution was observed as being turbid after soaking for 21 h at 50 °C. These results suggest that the hydrolysis reaction was promoted by the addition of $Sr(NO_3)_2$. The influence of $Sr(NO_3)_2$ on the hydrolysis of AHFT can be easily ascribed to the possible reactions of Sr^{2+} with F^- or any other hydrolysis product of AHFT, such as $[TiF_{6-n}(OH)_n]^{2-}$. SrF_2 is a familiar precipitate obtained by dissolving $SrCO_3$ in a HF aqueous solution, but it should be impossible in our solution system because our as-deposited film could be dissolved in HF aqueous solution again. Similarly, we can infer from the following two reasons that the Sr species present in our STO films should not be $SrCO_3$, which is usually generated when a strong alkaline solution of strontium salt is exposed to air. First, our solutions exhibited acidity (pH 3.4). Second, if $SrCO_3$ had formed, decomposition would require annealing at high temperatures, but no diffraction peak assigned to $SrCO_3$ was observed for our as-deposited thin film or those after annealing at 500 °C. Although the Fourier transform infrared (FTIR) measurement and thermogravimetric (TG) analysis suggested the formation of a trace of $SrCO_3$ under the present conditions, XPS results still showed that most of the Sr was present in a STO precursor solid phase.

We propose that Sr^{2+} reacting with $[TiF_{6-n}(OH)_n]^{2-}$ to form a compound of $Sr[TiF_{6-n}(OH)_n]$ is responsible for the stiochoimetry in terms of the Sr/Ti ratio of our films.[23] However, we should still consider why a TiO_2 peak was not observed even when the starting molar ratio of AHFT/SN/BA was 2:1:3 or 1:2:3.[23] In our previous experiments, the soaking time (12 h) was long enough and the annealing temperature (800 °C) was high enough to crystallize the Ti species if Ti existed separately and did not bind to the Sr through an oxygen bridge. No diffraction peaks related to TiO_2 appeared in the annealed powders collected after deposition of STO thin films. Hence, excessive Ti species should remain in the solution. For the solution with the starting molar ratio AHFT/SN/BA 2:1:3, according to the reaction equation (see the next section), the amount of BA added was enough for consumption of F^-, and we should clarify why the residual Ti species was not hydrolyzed to produce TiO_2 during the formation of STO.

For this purpose, we conducted new experiments, emphasizing the following trial on the excessive Ti species. Film obtained by depositing at 50 °C for 20 h in a solution with a molar ratio of AHFT/SN/BA 2:1:3 was amorphous (Figure 5a). After annealing at 800 °C for 1 h in air, only diffraction peaks attributed to STO were observed (Figure 5b). After the precipitate was filtered and the collected solution was soaked at 50 °C for another 20 h, the XRD analysis of the collected powder showed no peaks related to TiO_2 even after annealing (XRD profile not shown). After soaking for 40 h, small peaks of anatase TiO_2 were observed, indicating that anatase had formed (Figure 5c). After annealing at 800 °C, strong diffraction peaks of STO appeared (Figure 5d), suggesting that most of the as-collected powders were related to STO precursors, which

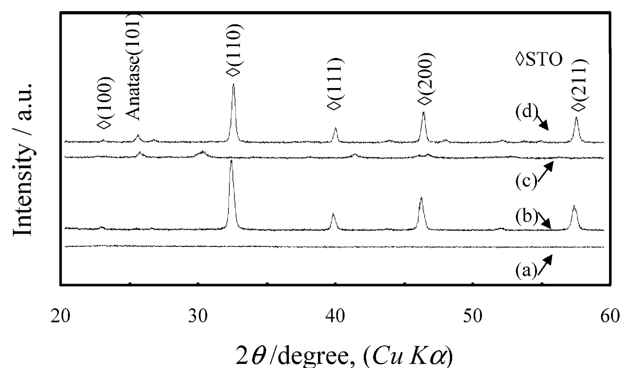

Figure 5. XRD profiles of the as-prepared STO precursor thin films and powders obtained in an AHFT/SN/BA 2:1:3 aqueous solution at 50 °C along with those annealed at 800 °C for 1 h in air: (a) the as-deposited thin film obtained by 20 h soaking; (b) the corresponding film of (a) after annealing; (c) the as-prepared powder collected for 40 h soaking by using a filtered solution of (a); and (d) the corresponding film of (c) after annealing.

were in an amorphous state. The precipitate was filtered and the residual solution was soaked at 50 °C for another 60 h. Almost no visual precipitation occurred, suggesting that the Ti species may have reacted completely before this stage. These experiments show the difference in reaction time necessary for the formation of the STO precursor solid and titania when Sr and Ti species coexisted in an aqueous solution; Ti species cannot hydrolyze smoothly to produce TiO_2, but do produce some intermediate forms that can react with Sr species; excessive Ti species began to hydrolyze to form TiO_2 after all Sr species were consumed. These results also imply that the formation energy for STO precursor is much lower than that for TiO_2 in the present system.

Our as-deposited STO thin films were stoichiometric in terms of Sr/Ti ratio, and control of the Sr/Ti ratio was easily achieved. This is very important in subjecting our films to practical applications. Comparably, some wet-chemical methods, i.e., MOCVD, have been reported for the synthesis of perovskite compounds including thin films and powders, but control of stoichiometric composition was difficult.[32]

Effect of Supersaturation on the Film Deposition. All depositions were accompanied by visible turbidity in the present work. The deposition solution remained clear for up to 30 min of soaking (0.025 M AHFT, AHFT/SN/BA 1:1:3 (molar ratio), 50 °C), which was shortened or prolonged slightly by changing the deposition temperature to 60 °C or 40 °C, respectively. By retaining the molar ratio of AHFT/SN/BA 1:1:3 and increasing the concentration of AHFT to 0.05 or 0.075 M, obvious precipitation occurred immediately even at room temperature after mixing. These findings suggest that hydrolysis reactions were accelerated by increasing temperature and molar concentration of the starting materials.

The relative amount of boric acid largely affected the reaction process of the solution. When the molar ratio

(32) (a) Kang, C. S.; Cho, H.-J.; Hwang, C. S.; Lee, B. T.; Lee, K.-H.; Horii, H.; Kim, W. D.; Lee, S. I.; Lee, M. Y. *Jpn. J. Appl. Phys.* **1997**, *36*, 6946. (b) Min, Y.-S.; Cho, Y. J.; Kim, D.; Lee, J.-H.; Kim, B. M.; Lim, S. K.; Lee, I. M.; Lee, W. I. *Chem. Vap. Deposition* **2001**, *7*, 146.

of AHFT/SN/BA was reduced from 1:1:3 to 1:1:1, the solution containing 0.025 M AHFT remained transparent even after 4 h, which was further extended to over 13 h if no boric acid was used. After 4 h, a turbid solution was obtained, remained turbid for 3−4 h, and then settled and the solution recovered to a clear state, indicating that homogeneous nucleation occurred dominantly during film deposition.

All these observations can be explained by the supersaturation degree of the solution, which was determined by the nature of the hydrolysis reaction. According to the usual theory of crystal growth,[33] no nucleation occurs in a solution with low supersaturation, homogeneous nucleation occurs at high supersaturation, and film formation via heterogeneous nucleation is possible in the intermediate supersaturation region called a "window." The precipitation of a solid phase involves four kinetic steps:[34] (1) formation of zero-charge precursor $Sr[TiF_{6-n}(OH)_n]$; (2) creation of nuclei; (3) growth of nuclei; and (4) aging of the particles in the suspension. For a monocation system, when the solution becomes supersaturated, the interaction between soluble precursor molecules generated by hydrolysis reaction drastically changes to be slightly attractive. This does not mean that all molecules clutch together immediately to form a solid. They continue moving, but a certain probability of collision could give rise to the formation of clusters of molecules, a solid phase. Whether the cluster can further grow or not is dominated by the relative energy state, exhibiting random fluctuation. Free energy difference between the liquid and the solid is the driving force toward the formation of a solid, whereas the surface tension results in redissolution of the existing clusters. Both of them are correlated with the radius of cluster. Once the radius of cluster is over a critical value, the total free energy begins to decrease and the stable nucleus is formed. Creation of nuclei occurs through the condensation of zero-charge precursor and is closely related to the precursor concentration. At the lower supersturation, the condensation rate is almost zero; once the precursor concentration exceeds a critical concentration C_{min}, the condensation rate increases abruptly and polynuclear entries − the nuclei − are formed in an explosive manner throughout the solution. Growth of nuclei follows the same chemical mechanism as nucleation.

The grain size, along with its distribution, is linked to the relative nucleation and growth rates. If the nucleation rate is much greater than the rate at which the new precursor is generated, nucleation does not occur simultaneously with the growth, and grains with narrow size distribution can be obtained. Conversely, if the nucleation rate is not high enough compared to the rate of precursor generation, the precursor concentration remains higher than C_{min}, and nucleation and growth occur simultaneously. The older nuclei will grow to be larger than the younger ones, leading to a wide grain-size distribution.

For our deposition solution, the hydrolysis product of AHFT may react with Sr^{2+} to form soluble new entries of $Sr[TiF_{6-n}(OH)_n]$, which further develop to clusters and nucleus. Although we cannot determine from the present results whether the first nuclei are generated in the solution or by the surface-promoted heterogeneous nucleation, films were mostly deposited in a turbid solution, which suggests that the formation of the solid was dominated by the homogeneous nucleation and attachment process; the particles seem to have formed by coalescence of very small particles rather than by direct nuclei growth on the SAM surface. This can be clearly observed in the initial stage of deposition by both SEM[23] and AFM. As shown in Figure 3 A1 and B1, we can observe grains with a wide range of size distribution; the smallest particle is less than 10 nm, while the largest one aggregated by several smaller ones is about 50 nm. With deposition proceeding from 5 to 6 h, the size distribution became narrow and the mean particle size increased slightly, suggesting that the smaller particles were scavenged by the larger ones.

The whole film was composed of small particles, which can be observed in a cross-sectional FE-SEM photograph (Figure 6a) and an AFM image (Figure 6b). Realization of a hundreds-of-nanometers-thick film by the traditional chemical solution method, i.e sol−gel, usually needs multiple cycles of deposition and firing, whereas a single-layer thickness about tens of nanometers thick is achieved by using solutions of low viscosity. Evidently, this is time-consuming and complicated for industrial applications. However, using the present method, a crack-free dense film about 480 nm thick was prepared on the UV-irradiated OTS−SAM surface by a single-step deposition. The film showed particulate microstructure; particles of 20−50 nm in diameter were closely packed on the cross-sectional surface and no cavities or cracks were observed in either the plane or cross-sectional surface. On the basis of AFM observation (see Figure 6b), both RMS (1.8 nm) for the entire measured area (500×500 nm^2) and the largest roughness (5.0 nm) in a cross-sectional roughness profile were much smaller than the film thickness (480 nm), confirming the formation of a smooth particulate surface. After annealing at 600 °C for 1 h in air (Figure 6c and d), shrinkage occurred and small particles of about 10-nm diameter were clearly observed in the surface. However, the surface remained smooth.

We thus inferred that the chemical interaction between nuclei and the substrate surface dominated the attachment of homogeneous nuclei to the substrate in the initiate stage. With deposition proceeding, possibly also correlated to the coverage or grain size, the attachment of nuclei was driven by the interaction between nuclei and deposited grains on the substrate, following the "Ostwald Ripening" mechanism; that is, larger particles grow through consumption of smaller ones. However, heterogeneous nucleation still occurred at low pH, suggesting that the supersaturation degree was closely dependent on pH (Figure 4). In any case, the supersaturation should be maintained for a period sufficient to deposit the solid phase.

The effect of solution conditions on the supersaturation degree can be understood by merely considering the hydrolysis reaction. Hydrolysis reactions of dissociated

(33) (a) Sawada, K. In *Crystallization Process*; Ohtaki, H., Ed.; John Wiley & Sons: Chichester, U.K., 1998. (b) Saito, N.; Haneda, H.; Seo, W. S.; Koumoto, K. *Langmuir* **2001**, *17*, 1461.

(34) (a) Jolivet, J.-P.; Henry, M.; Livage, J. *Metal Oxide Chemistry and Synthesis*; John Willey & Sons: Chichester, U.K., 2000; pp 37−52. (b) Sugimoto, T. *Adv. Colloid Interface Sci.* **1987**, *28*, 65.

Figure 6. FE-SEM photograph (a) and AFM image (b) of a STO precursor thin film deposited on the OTS-derived silanol surfaces. The film was prepared in a 25 mM AHFT, 25 mM SN, and 75 mM BA aqueous solution for 24 h. (c) AFM image of the same specimen after annealing at 600 °C for 1 h in air and (d) enlarged AFM image of (c). The roughness profile of a cross-sectional surface indicated by a line is also shown.

AHFT salt in the presence of HBO_3 can be represented as follows:

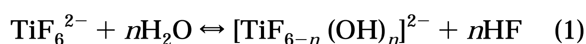

$$TiF_6^{2-} + nH_2O \Leftrightarrow [TiF_{6-n}(OH)_n]^{2-} + nHF \quad (1)$$

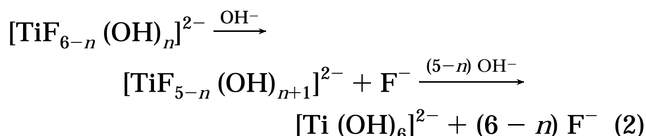

$$[TiF_{6-n}(OH)_n]^{2-} \xrightarrow{OH^-} [TiF_{5-n}(OH)_{n+1}]^{2-} + F^- \xrightarrow{(5-n)\,OH^-} [Ti(OH)_6]^{2-} + (6-n)F^- \quad (2)$$

and promotion of hydrolysis by BA:

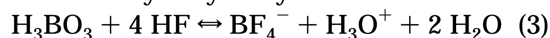

$$H_3BO_3 + 4\,HF \Leftrightarrow BF_4^- + H_3O^+ + 2\,H_2O \quad (3)$$

As shown in eqs 1 and 2, hydrolysis of TiF_6^{2-} takes place by a ligand-exchange reaction.[23] Although the degree of hydrolysis for eq 1 is low and decreases with increasing concentration of TiF_6^{2-}, the product HF can be scavenged by H_3BO_3 immediately; the reaction proceeds stepwise, and one of them is shown in eq 3, which accelerates eq 1 and shifts the equilibrium to the right-hand side. As this is an endothermic reaction, raising the temperature can promote the hydrolysis

(35) (a) Öner, D.; McCarthy, T. J. *Langmuir* **2000**, *16*, 7777. (b) Krüger, C.; Jonas U. *J. Colloid Interface Sci.* **2002**, *252*, 331.

reaction and increase the supersaturation degree, resulting in a smaller size of critical nuclei and high nucleation rate. In contrast, at lower temperatures, critical nuclei with a larger size are needed, and hence nucleation and growth are suppressed. With the supersaturation degree increasing and the precursor concentration exceeding a critical concentration of C_{min}, nuclei begin to form, but because the precursor concentration is still close to C_{min}, the precursors condense preferentially on existing nuclei, causing them to grow. Some of these nuclei are further attracted to the particles on the substrate. This explanation is consistent with the experimental results showing grain size decreasing with increasing temperature of deposition solution.

Equations 1 and 3 clearly reveal that the hydrolysis reaction of AHFT will produce a weak acid HF and HBF_4, which increases the acidity of the solution. Hence, lowering the pH suppresses the hydrolysis reaction and decreases the supersaturation degree, which makes heterogeneous nucleation possible. As shown in Figure 4, needlelike crystals were formed on the substrate, but were not observed in the precipitate collected from the bottom of the beaker.

Effect of Surface Functionality. Adsorption of charged particles on oppositely charged surfaces, such as double-helix DNA, actin, charged colloids, charged membranes, or any charged interfaces, is of growing importance because it provides a route to the production of chemically or biologically active substrates[35] and optical or electronic devices.[36] SAMs can modify the surface of a substrate with required charges for the deposition of charged colloid particles. Aizenberg et al.[15b] used substrates of micropatterned SAMs with anionic and cationic regions to govern the deposition of charged colloid particles. The driving forces of the adsorption process are long-range electrostatic forces, i.e., attraction interactions between functional groups on the particle surfaces and the molecular layers of the substrate. Besides specific molecular interactions, capillary forces play an important role in the assembly process. We studied site-selective adhesion of hydroxyapatite (HAp) microparticles to charge-micropatterned SAMs.[37] At controlled pH, negatively charged HAp particles selectively attached to the positively charged amino regions compared to negatively charged silanol regions. De Guire et al.[12,38] and other researchers[11,14] found that sulfated surfaces could effectively enhance formation of uniform and adherent thin films. They attributed this to the relatively strong interaction between sulfated SAMs and grains in the solution.

However, there are still certain phenomena that cannot be explained by the proposed electrostatic interaction mechanism. For example, in the LPD-deposited TiO_2,[4] we found that silanol surfaces produced adherent films at pH 2.88. Under such conditions, TiO_2 particles are positively charged (isoelectric point: 4−5;[39] 4;[40] 5.5[41]). Although no zeta potential value of UV-irradiated SAM (silanol) surface at pH 3.4 is available, ideally, both a cleaned Si wafer with a native silica layer and an UV-irradiated SAM surface are covered with the silanol groups. The zeta potential of a Si wafer was practically measured (Figure 7). Although the isoelectric point was found to be higher than the reported value (pH 2.0[42]), it was still suggested that the silanol surface was positively charged or close to neutral at pH 3.4. A potential measurement for a STO precursor solid and a Si wafer are shown in Figure 7; the isoelectric point for the STO precursor solid was obtained at pH 5.1, suggesting that a STO precursor solid holds positive charges. So both STO/TiO_2 and the silanol surface were positively charged, suggesting that the thin film could not have formed based on electrostatic interactions between nuclei or grains and substrate surfaces, which is a conclusion contradictory to our experimental observation. Similar findings have also been obtained when employing silanol surfaces to prepare TiO_2 thin films in an organic solution[5,6] or through a gas phase.[21] These results reveal the complexity of the chemical deposition process, indicating the interdependence of solution conditions and surface functionalities, and implying different mechanisms would operate in different systems.

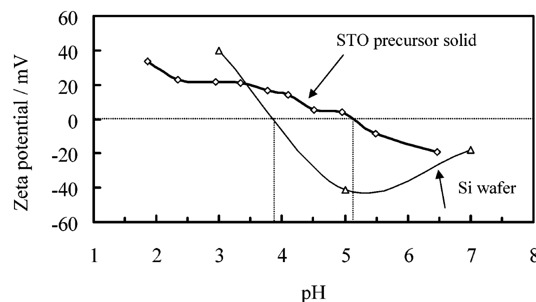

Figure 7. Zeta potential of STO precursor solid and cleaned Si wafer.

We found that films on the silanol surfaces showed strong adherence in the Scotch tape adhesion peel test. For the as-deposited STO precursor thin film, peeled fragments were not found. Films could not be completely torn off even after strongly rinsing by ultrasonication (150 W) for as long as 30 min. The strong adhesion of films on the silanol regions was thus attributed to chemical bonds formed between STO precursor particles and OH groups of silanol regions by condensation. Such a chemical bond formation would not occur on hydrophobic regions, such as octadecyl, amino, and phenyl surfaces, resulting in relatively weak adhesion strengths. However, the mechanism proposed here for selective deposition of STO might be different from that for TiO_2 deposited in a toluene solution of titanium dichloride diethoxide (TDD),[6b] where, as we suggested, the solvated hydroxo species formed by the hydrolysis of TDD reacted with hydroxo groups of the silanol surface by

(36) (a) Roxlo, C. B.; Deckman, H. W.; Gland, J.; Cameron, S. D.; Chianelli, R. R. *Science* **1987**, *235*, 1629. (b) Burmeister, F.; Schäfle, C.; Matthes, T.; Böhmisch, M.; Boneberg, J.; Leiderer, P. *Langmuir* **1997**, *13*, 2987.

(37) (a) Zhu, P. X.; Masuda, Y.; Koumoto, K. *J. Colloid Interface Sci.* **2001**, *243*, 31. (b) Zhu, P. X.; Ishikawa, M.; Seo, W. S.; Koumoto, K. *J. Biomed. Mater. Res.* **2002**, *59*, 294.

(38) (a) Shin, H.; Collins, R. J.; De Guire, M. R.; Heuer, A. H.; Sukenik, C. N. *J. Mater. Res.* **1995**, *10*, 692. (b) Supothina, S.; De Guire, M. R. *Thin Solid Films* **2000**, *371*, 1.

(39) Subramaniam, K.; Yiacoumi, S.; Tsouris, C. *Colloid Surf. A* **2000**, *177*, 133.

(40) Gun'ko, V. M.; Zarko, V. I.; Chibowski, E.; Dudnik, V. V.; Leboda, R. V.; Zaets, A. *J. Colloid Interface Sci.* **1997**, *188*, 39.

(41) Yang, H. G.; Li, C. Z.; Gu, H. C.; Fang, T. N. *J. Colloid Interface Sci.* **2001**, *236*, 96.

(42) Hozumi, A.; Sugimura, H.; Yokogawa, Y.; Kameyama, T.; Takai, O. *Colliod Surf. A* **2001**, *182*, 257.

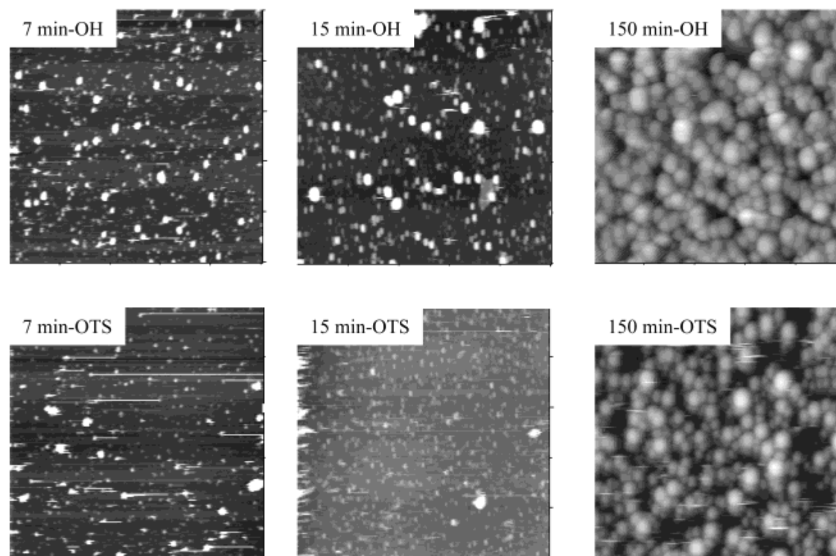

Figure 8. AFM images of deposits on the OTS-derived silanol surfaces (upper row) and OTS (lower row) surfaces after soaking in a 0.025 M AHFT, 0.025 M SN, and 0.075 M aqueous solution for 7, 15, and 150 min (from left to right), respectively. The measured areas were 500 × 500 nm^2.

condensation, constructing Ti−O−Si bridges. The open structure of soluble hydroxo species (free OH groups) enables condensation between them and fabrication of a Ti−O−Ti skeleton. On the basis of this proposal, TiO_2 thin films of any thicknesses can be prepared so long as the required supersaturation is maintained, and the film should exhibit strong adherence to the substrate.

For the STO thin film, thickness of the film showing strong adhesion is limited to less than about 480 nm. The reason lies not only in the fast hydrolysis rate but also in the different formation mechanism. As the hydrolysis of AHFT proceeds much more quickly in the presence of $Sr(NO_3)_2$, solutions with high supersaturation could be maintained for only a short period of time, which in turn influences the deposition process and results in thinner films. Hence, we assume that chemical bond formation was taking place in the initial monolayer. After this layer has formed, electrostatic forces may dominate the deposition process. The weak adhesion of thick film may be attributed to the mismatch of structure or thermal expansion coeffecient difference between the deposit and the substrate.

The deposition process in the hydrophilic and hydrophobic surface was investigated by using OTS surface and OTS-derived silanol surface, emphasizing comparing their different growth rates. As shown in Figure 8, although the difference in amount of deposit on the OTS and OTS-derived silanol surfaces is not so obvious, the deposition rate on the hydrophilic silanol regions was still higher than that on the hydrophobic OTS regions. After soaking for 1.5 h, a dense 90-nm-thick film was obtained on the silanol surface. However, in the film on the OTS surface, about 52 nm thick as measured by ellipsometer, cavities were clearly observed. These results suggest that the deposition was promoted on the hydrophilic surface. The similar conclusion has been drawn when we prepared a STO precursor thin film on the HFDTS and HFDTS-derived silanol surfaces.[23]

Now we should consider the deposition that occurs on the UV-irradiated different SAMs. Generally, the surface properties are affected by the type, size, and structure of SAMs.[43] Photocleavage resulted in the decomposition of carbon−hydrogen chains of SAMs and reconstruction of silanol groups for some SAMs, such as PTCS.[44] However, the strong deep UV absorption of the phenyl chromophore renders PTCS films susceptible to patterning via Si−C bond photocleavage at lower exposure doses than those obtained for simple alkylsiloxanes (e.g., ~350 mJ/cm^2 for PTCS vs > 20 J/cm^2 for octadecylsiloxane SAMs at 193 nm[4,20a]). Different photochemistries of OTS and PTCS are due to different absorption cross-sections associated with different molecular structures.[20] Although a concrete understanding of the transition mechanism is not included in the present work, properties such as the wetting sensitivity of obtained functional silanol groups to surface chemistry has been reported to be affected by the relative concentration of OH and CH_3.[45] In the present research, SAMs were exposed to UV light for a specific time, usually 2 h, to achieve photocleavage. The water-contact angle of silanol surface derived from OTS−SAM was a little larger than that from PTCS−SAM (10° vs 6°), indicating that it is still possible for a concentration difference of OH and CH_3 to occur after UV irradiation for the same length of time, due to the molecular structure difference of these two SAMs, which may be responsible for the slight changes in film morphology.

5. Conclusions

We prepared $SrTiO_3$ (STO) precursor thin films on different self-assembled monolayer (SAM) surfaces in an aqueous solution of $(NH_4)_2TiF_6/Sr(NO_3)_2/H_3BO_3$ at low temperatures (40−60 °C). The morphology, growth rate, growth mechanism, and growth kinetics of the film were investigated. The uniform, smooth, and adhesive films with thickness in the range of 25−480 nm could be prepared on the OH-group-terminated surfaces, which were obtained by exposure of SAM-covered Si

(43) Ulman, A. *Chem. Rev.* **1996**, *96*, 1533.
(44) Dulcey, C. S.; Georger, J. H.; Krauthamer, V.; Stenger, D. A.; Fare, T. L.; Calvert, J. M. *Science* **1991**, *252*, 551.
(45) Ulman, A.; Evans, S. D.; Shnidman, Y.; Sharma, R.; Eilers, J. E.; Chang, J. C. *J. Am. Chem. Soc.* **1991**, *113*, 1499.

substrates to the UV light. Films with almost similar quality could be prepared on both phenyltrichlorosilane (PTCS) and PTCS-derived silanol surfaces. The film was transparent and composed of closely packed nanosized grains on these surfaces; a grain size range of 20−50 nm was observed by AFM. This characteristic was observed not only in the surface of the film, but also in sectional surfaces. The slight change in morphology of the different SAM-derived silanol surfaces was due to differences in the nature of the SAMs. Both SEM and AFM observation of the initiatial deposition stage suggest that the homogeneous nucleation and attachment process dominated the deposition of solid in most cases; the grains appear to have formed by coalescence of very small ones rather than by direct nuclei growth. Therefore, the supersaturation degree of the solution had a great effect on the film deposition. Higher deposition temperature or pH increased supersaturation of the solution, resulting in higher growth rate and smaller grain size. However, thin films deposited at lower pH were opaque and showed low density and different morphology; films were composed of brush-like aggregates of unidentified crystallized fibers, which could be transformed to perovskite-type STO after annealing at 600 °C in air. A comparative study on deposition of TiO_2 and STO by the LPD method was conducted, and control of STO film composition in stoichiometry was also discussed. The results showed a time difference between the deposition of STO and TiO_2 with the coexistence of Sr and Ti species; STO was preferably produced first. Hence, a stoichiometric film was easily synthesized by the present method.

Acknowledgment. We express our gratitude to Dr. Y.-Y. Wu for her kind help in FE-SEM observation. T. Nakanishi is thanked for the supporting data of zeta potential. We acknowledge Drs. N. Shirahada and P.-X. Zhu for their critical reading of the manuscript. Y.-F.G. is grateful to NGK Insulators Ltd. of Japan for supporting a scholarship.

CM030234S